

# Evaluating study of the momentum and heat exchange process of two surface layer schemes during severe haze pollution in Jing-Jin-Ji in east China

Yue Peng<sup>1,2</sup>, Hong Wang<sup>1,2</sup>, Yubin Li<sup>3</sup>, Changwei Liu<sup>3</sup>, Tianliang Zhao<sup>2</sup>, Xiaoye Zhang<sup>1</sup>, Zhiqiu Gao<sup>3,4</sup>, Tong Jiang<sup>5</sup>, Huizheng Che<sup>1</sup>, Meng Zhang<sup>6</sup>

<sup>1</sup> State Key Laboratory of Severe Weather/Institute of Atmospheric Composition, Chinese Academy of Meteorological Sciences (CMAS), Beijing 100081, China

<sup>2</sup> Collaborative Innovation Center on Forecast and Evaluation of Meteorological Disasters/Key Laboratory for Aerosol-Cloud-Precipitation of China Meteorological Administration, Nanjing University of Information Science and Technology, Nanjing 210044, China

<sup>3</sup> Key Laboratory of Meteorological Disaster of Ministry of Education/Collaborative Innovation Center on Forecast and Evaluation of Meteorological Disasters, School of Remote Sensing and Geomatics Engineering, Nanjing University of Information Science and Technology, Nanjing 210044, China

<sup>4</sup> State Key Laboratory of Atmospheric Boundary Layer Physics and Atmospheric Chemistry, Institute of Atmospheric Physics, Chinese Academy of Sciences, Beijing 100029, China

<sup>5</sup> National Climate Center, China Meteorological Administration, Beijing 100081, China

<sup>6</sup> Beijing Meteorological Service, Beijing 100089, China

*Correspondence to:* Hong Wang (wangh@cma.gov.cn)

**Abstract.** The turbulent flux parameterization schemes in the surface layer are crucial for air pollution modeling. Pollutants prediction by atmosphere chemical model exists obvious deficiencies, which may be closely related to the uncertainties of the momentum and sensible heat fluxes calculated in the surface layer. The differences of two surface layer schemes (the Li and MM5 scheme) were discussed and the performance of the two schemes focusing on a heavy haze episode was mainly evaluated based on the observed momentum and sensible heat fluxes in Jing-Jin-Ji in east China. The results showed that the aerodynamic roughness length  $z_{0m}$  and the thermal roughness length  $z_{0h}$  play a major role in the flux calculation. Compared with the Li scheme, ignoring the difference between the two in the MM5 scheme induced a great error in the calculation of sensible heat flux (e.g., the error was 54 % at Gucheng station). Besides the roughness lengths, the algorithms of universal functions for surface turbulent fluxes as well as the roughness sublayer also resulted in certain errors in the MM5 scheme. In addition, magnitude of  $z_{0m}$  and  $z_{0h}$  has significant influence on the two schemes. The large  $z_{0m}$  and  $z_{0m}/z_{0h}$  in megacity with rough surface (e.g., Beijing) resulted in much larger differences of momentum and sensible heat fluxes by Li and MM5, compared with the small  $z_{0m}$  and  $z_{0m}/z_{0h}$  in suburban area with smooth surface (e.g., Gucheng). The Li scheme better characterized the evolution of atmospheric stratification than the MM5 scheme in general, especially for the transition stage from unstable to stable atmospheric stratification corresponding to the  $PM_{2.5}$  accumulation. The bias of momentum and sensible heat fluxes from Li were lower about 38 % and 43 % respectively than those from MM5 during this stage. This study indicates the superiority of the Li scheme in the describing of the regional atmospheric stratification, and also suggests the improving

35 possibility of severe haze prediction in Jing-Jin-Ji in east China by coupling it into the atmosphere chemical model online.

36 **Key words:** surface layer; turbulent flux parameterization; roughness length; numerical modeling; air pollution

## 37 **1 Introduction**

38 Adequate air quality modeling relies on accurate simulation of meteorological conditions, especially in the planetary  
39 boundary layer (PBL) (Hu et al., 2010; Cheng et al., 2012; Xie et al., 2012). The PBL is tightly coupled to the earth's surface  
40 by turbulent exchange processes. As the bottom layer of PBL, the surface layer (SL) reflects the surface state by calculating  
41 momentum, heat, water vapor and other fluxes, and influences the atmospheric structure by turbulent transport process. Many  
42 studies have illustrated the important roles of meteorological factors in the SL in the formation of air pollution. They  
43 demonstrated that weak wind speed, high relative humidity (RH) and strong temperature inversion are favorable for the haze  
44 concentrating (Zhang et al., 2014; Yang et al., 2015; Liu et al., 2017; Zhong et al., 2017). The strong stable stratification and  
45 weak turbulent are mainly responsible for many haze events. The relationship between flux and atmospheric profile in the  
46 atmospheric surface layer is a critical factor for air pollution diffusion, especially under stable stratification conditions (Li et  
47 al., 2017). However, the study of stable boundary layer still has some uncertainties due to the poor description of surface  
48 turbulent motion. The simulating study on a severe haze in east China by the Weather Research and Forecasting/Chemistry  
49 (WRF-Chem) model concluded that there is lower ability of current PBL schemes in distinguishing the diffusion between haze  
50 days under stable condition and clean days under unstable condition (Li et al., 2016a). Another study (Vautard et al. 2012) on  
51 mesoscale meteorological models also pointed out a systematic overestimation of near-surface wind speed in a stable boundary  
52 layer and its possible contribution to the underestimation of the PM<sub>2.5</sub> pollution. In addition, atmospheric conditions in both  
53 the PBL and upper layers are highly dependent on the turbulent fluxes which are computed in the SL (Ban et al., 2010). Flux  
54 parameterization in the SL plays an important role in studies of the hydrological cycle and weather prediction (Yang et al.,  
55 2001; Li, 2014). An adequate SL scheme is crucial to provide an accurate atmospheric evolution by numerical models (Jiménez  
56 et al., 2012) and hence it may introduce significant impacts on air pollution simulation.

57 The bulk aerodynamic formulation based on Monin-Obukhov similarity theory (hereinafter MOST, Monin and Obukhov,  
58 1954) is usually employed to calculate surface fluxes in numerical models. Turbulent fluxes are parameterized by wind,  
59 temperature, humidity in the lowest layer in the model and temperature and humidity at the surface. Many international scholars  
60 verified the MOST using field experiments and then proposed the universal functions, the commonly used of which is  
61 Businger-Dyer (BD) equation (Businger, 1966; Dyer, 1967). With the development of observation technology, the coefficients  
62 in the BD equation have been further modified (Paulson, 1970; Webb, 1970; Businger et al., 1971; Dyer, 1974; Högström,  
63 1996). In addition to the BD equation, some other schemes have been put forward and they performed better especially for  
64 strongly stable stratification (Holtslag and De Bruin, 1988; Beljaars and Holtslag, 1991; Cheng and Brutsaert, 2005). The

65 schemes can be divided into two types according to the computing characteristics. One type is called as iterative algorithm  
66 (Paulson, 1970; Businger et al., 1971; Dyer, 1974; Högström, 1996; Beljaars and Holtslag, 1991), and it keeps the MOST  
67 completely with less approximation so that the results can be more precise. However, it needs to take much more steps to  
68 converge and hence the CPU time is consuming which reduces the computational efficiency of modeling (Louis, 1979; Li et  
69 al., 2014); The other one is called as non-iterative algorithm (Louis et al., 1982; Launiainen, 1995; Wang et al., 2002; Wouters  
70 et al., 2012). There is no requirement for loop iteration in the calculation due to the approximate treatment. This algorithm is  
71 much simpler and less CPU time-consuming, but the results are based on the loss of the calculation accuracy.

72 A new non-iterative scheme proposed by Li et al. (2014; 2015, Li hereinafter) speeds up effectively under a higher  
73 accuracy compared with some classic iterative computation. It is remarkable that this new scheme just has been theoretically  
74 evaluated and it has never been applied in any models. Haze pollution occurs frequently in recent years in east China. The  
75 concentration of PM<sub>2.5</sub> may reach up to 1000  $\mu\text{g m}^{-3}$  in the Beijing-Tianjin-Hebei (Jing-Jin-Ji) region in winter (Wang et al.,  
76 2014) while it was generally underestimated by current air quality models (Zhang et al., 2015; Li et al., 2016a; Liu et al., 2017).  
77 The Li and another classic SL scheme (Zhang and Anthes, 1982, MM5 hereinafter) are compared in details in this study. The  
78 observed momentum and sensible heat flux data covering one complete haze process at Gucheng station were used to evaluate  
79 the two schemes focusing on the transition stage from unstable to stable atmospheric stratification corresponding to the PM<sub>2.5</sub>  
80 accumulation. The evaluation is in the view of both local and regional scales. This offline study may provide the prerequisite  
81 for the online coupling the Li scheme into atmosphere chemical model in the future.

## 82 **2 Theory**

83 The definition of momentum and sensible heat flux as well as the detailed algorithms of the Li and MM5 schemes are  
84 introduced in this section.

### 85 **2.1 Introduction of the momentum and sensible heat flux**

86 The turbulent fluxes from ground surface are defined as follows:

$$87 \tau = \rho u_*^2, \quad (1a)$$

$$88 H = -\rho c_p u_* \theta_*, \quad (1b)$$

89 where  $\tau$  is the momentum flux,  $H$  is the sensible heat flux,  $\rho$  is the air density,  $c_p$  is the specific heat capacity at constant  
90 pressure.  $u_*$  and  $\theta_*$  are the friction velocity and the temperature scale, respectively, and they represent the intensity of the  
91 vertical turbulent flux transport and are approximately independent on height in the SL.

92 Both the Li and MM5 schemes are calculated with bulk flux parameterization. As an important dimensionless parameter  
93 related to the stability, the bulk Richardson number  $Ri_B$  is defined as

94 
$$Ri_B = \frac{gz(\theta - \theta_g)}{\theta u^2}, \quad (2)$$

95 where  $g$  is the acceleration of gravity,  $z$  is the reference height which is the lowest level in the model,  $\theta$  is the mean potential  
 96 temperature at height  $z$ ,  $\theta_g$  is the surface radiometric potential temperature,  $u$  is the mean wind speed at height  $z$ . Thus,  $Ri_B$   
 97 can be computed through meteorological variables from at least two levels.

## 98 2.2 The Li scheme

99 This new scheme employs non-iterative algorithm to compute the surface fluxes. Its basic idea is to parameterize the  
 100 stability parameter  $\zeta$  directly with  $Ri_B$  and roughness lengths ( $z_{0m}$  and  $z_{0h}$ ). Specifically, bulk transfer coefficients of the  
 101 momentum and sensible heat fluxes ( $C_M$  and  $C_H$ ) are expressed as

102 
$$C_M = \frac{u_*^2}{u^2} = \frac{\tau}{\rho u^2}, \quad (3a)$$

103 
$$C_H = \frac{u_* \theta_*}{u(\theta - \theta_g)} = -\frac{H}{\rho c_p u(\theta - \theta_g)}. \quad (3b)$$

104 Based on MOST and considering the roughness sublayer (RSL) effect at the same time, the relationships between the  
 105 bulk transfer coefficients and the profile functions corresponding to wind and potential temperature are usually expressed as

106 
$$C_M = \frac{k^2}{\left[ \ln \frac{z}{z_{0m}} - \psi_M \left( \frac{z}{L} \right) + \psi_M \left( \frac{z_{0m}}{L} \right) + \psi_M^* \left( \frac{z}{L}, \frac{z}{z_*} \right) \right]^2}, \quad (4a)$$

107 
$$C_H = \frac{k^2}{R \left[ \ln \frac{z}{z_{0m}} - \psi_M \left( \frac{z}{L} \right) + \psi_M \left( \frac{z_{0m}}{L} \right) + \psi_M^* \left( \frac{z}{L}, \frac{z}{z_*} \right) \right] \left[ \ln \frac{z}{z_{0h}} - \psi_H \left( \frac{z}{L} \right) + \psi_H \left( \frac{z_{0h}}{L} \right) + \psi_H^* \left( \frac{z}{L}, \frac{z}{z_*} \right) \right]}, \quad (4b)$$

108 where  $k$  is the von Kármán constant which is 0.4 in both two schemes,  $R$  is the Prandtl number which is 1.0 in the two  
 109 schemes,  $z_{0m}$  and  $z_{0h}$  are the aerodynamic roughness length and the thermal roughness length, respectively.  $\psi_M$  and  $\psi_H$   
 110 are the integrated stability functions for momentum and sensible heat, respectively, which are also called universal functions.

111  $L$  is the Obukhov length ( $\zeta = \frac{z}{L}$ ),  $\psi_M^*$  and  $\psi_H^*$  are the correction functions accounting for RSL effect,  $z_*$  is the RSL height.

112 It is clear to see that the calculation of the momentum and sensible heat fluxes requires  $C_M$  and  $C_H$  (or  $u_*$  and  $\theta_*$ ), and  
 113 there are 3 key points to get them:

- 114 1.  $z_{0m}$  and  $z_{0h}$ .  $z_{0m}$  and  $z_{0h}$  are two key parameters in the bulk transfer equations. Their definitions and influence  
 115 will be discussed in Sect. 4.1. Note that both  $z_{0m}$  and  $z_{0h}$  are taken into account by the Li scheme. In other words, the  
 116 Li scheme distinguishes these two principal surface parameters effectively as they generate from different mechanisms.
- 117 2.  $\zeta$ . The determination of  $\zeta$  is the most crucial problem for the Li scheme. In fact, this new scheme consists of two  
 118 parts. The first part was proposed for atmospheric stable stratification condition (Li et al., 2014), and the second part then  
 119 extended the scheme to unstable condition (Li et al., 2015). For stable condition, the calculation procedure for a given  
 120 group of  $Ri_B$ ,  $z_{0m}$  and  $z_{0h}$  is the following: (1) find the region according to  $z_{0m}$  and  $z_{0h}$ ; (2) find the section  
 121 according to the region and  $Ri_B$  with Eq. (5) and given coefficients; (3) calculate  $\zeta$  using Eq. (6) and given coefficients.

122 
$$Ri_{Bcp} = \sum C_{mn} (\log L_{0M})^m (L_{0H} - L_{0M})^n, \quad (5)$$

123 
$$\zeta = Ri_B \sum C_{ijk} Ri_B^i L_{0M}^j (L_{0H} - L_{0M})^k, \quad (6)$$

124 where  $C_{mn}$  and  $C_{ijk}$  are the coefficients in Tables in Li et al. (2014).  $L_{0M} = \ln \frac{z}{z_{0m}}$ ,  $L_{0H} = \ln \frac{z}{z_{0h}}$ .  $m, n = 0, 1, 2$ , and  
 125  $m + n \leq 3$ ;  $i, j, k = 0, 1, 2, 3$ , and  $i + j + k \leq 4$ . Similarly, for unstable condition, eight regions are divided according  
 126 to the method from Li et al. (2015). For each of the regions,  $\zeta$  is carried out by following:

127 
$$\zeta = Ri_B \frac{L_{0M}^2}{L_{0H}} \sum C_{ijk} \left( \frac{-Ri_B}{1-Ri_B} \right)^i L_{0M}^{-j} L_{0H}^{-k}, \quad (7)$$

128 where  $C_{ijk}$  is listed in Li et al. (2016b), and  $i = 0, 1$ ;  $j, k = 0, 1, 2, 3$ ;  $i + j + k \leq 4$ .

129 3. Universal function. It is also a key factor in flux calculation. The form of universal function here is adopted from Cheng  
 130 and Brutsaert (2005) under the stable condition (Eqs. (8a), (8b)) and it is adopted from Paulson (1970) under the unstable  
 131 condition (Eqs. (9a), (9b)):

132 
$$\psi_M(\zeta) = -a \ln \left[ \zeta + (1 + \zeta^b)^{\frac{1}{b}} \right], \quad \zeta > 0 \text{ (stable)}, \quad (8a)$$

133 
$$\psi_H(\zeta) = -c \ln \left[ \zeta + (1 + \zeta^d)^{\frac{1}{d}} \right], \quad \zeta > 0 \text{ (stable)}, \quad (8b)$$

134 
$$\psi_M(\zeta) = 2 \ln \frac{1+x}{2} + \ln \frac{1+x^2}{2} - 2 \arctan(x) + \frac{\pi}{2}, \quad \zeta < 0 \text{ (unstable)}, \quad (9a)$$

135 
$$\psi_H(\zeta) = 2 \ln \frac{1+y}{2}, \quad \zeta < 0 \text{ (unstable)}, \quad (9b)$$

136 where  $a = 6.1$ ,  $b = 2.5$ ,  $c = 5.3$ ,  $d = 1.1$ ,  $x = (1 - 16\zeta)^{1/4}$ ,  $y = (1 - 16\zeta)^{1/2}$ .

137 In addition, the RSL effect is taken into account in the Li scheme. The definitions and influence of RSL will also be  
 138 discussed in Sect. 4.1. De Ridder (2010) proposed the expression of  $\psi_M^*$  and  $\psi_H^*$ :

139 
$$\psi_M^* \left( \zeta, \frac{z}{z_*} \right) = \phi_M \left[ \left( 1 + \frac{v}{\mu_{MZ}/z_*} \right) \zeta \right]^{\frac{1}{\lambda}} \ln \left( 1 + \frac{\lambda}{\mu_{MZ}/z_*} \right) e^{-\mu_{MZ}/z_*}, \quad (10a)$$

140 
$$\psi_H^* \left( \zeta, \frac{z}{z_*} \right) = \phi_H \left[ \left( 1 + \frac{v}{\mu_{HZ}/z_*} \right) \zeta \right]^{\frac{1}{\lambda}} \ln \left( 1 + \frac{\lambda}{\mu_{HZ}/z_*} \right) e^{-\mu_{HZ}/z_*}, \quad (10b)$$

141 where  $v = 0.5$ ,  $\mu_M = 2.59$ ,  $\mu_H = 0.95$ ,  $z_* = 16.7z_{0m}$ ,  $\lambda = 1.5$ .  $\phi_M$  and  $\phi_H$  are universal functions before  
 142 integration. Here, set  $\chi_M = 1 + \frac{v}{\mu_{MZ}/z_*}$ ,  $\chi_H = 1 + \frac{v}{\mu_{HZ}/z_*}$ :

143 
$$\phi_M(\chi_M \zeta) = 1 + a \frac{\chi_M \zeta + (\chi_M \zeta)^b [1 + (\chi_M \zeta)^b]^{\frac{1-b}{b}}}{\chi_M \zeta + [1 + (\chi_M \zeta)^b]^{\frac{1}{b}}}, \quad \zeta > 0 \text{ (stable)}, \quad (11a)$$

144 
$$\phi_H(\chi_H \zeta) = 1 + c \frac{\chi_H \zeta + (\chi_H \zeta)^d [1 + (\chi_H \zeta)^d]^{\frac{1-d}{d}}}{\chi_H \zeta + [1 + (\chi_H \zeta)^d]^{\frac{1}{d}}}, \quad \zeta > 0 \text{ (stable)}, \quad (11b)$$

145 
$$\phi_M(\chi_M \zeta) = (1 - 16\chi_M \zeta)^{-1/4}, \quad \zeta < 0 \text{ (unstable)}, \quad (12a)$$

146 
$$\phi_H(\chi_H \zeta) = (1 - 16\chi_H \zeta)^{-1/2}, \quad \zeta < 0 \text{ (unstable)}. \quad (12b)$$

147 **2.3 The MM5 scheme**

148 The MM5 scheme is a classic one which is widely applied in modeling investigation (Hu et al., 2010; Wang et al., 2015a,

149 b; Tymvios et al., 2017). This scheme does not distinguish  $z_{0h}$  from  $z_{0m}$ , thus the roughness length here is expressed as  $z_0$ .  
 150 For unstable condition, the function forms are given by Eqs. (16a) and (16b) following Paulson (1970), and for stable condition,  
 151 the atmospheric stratification conditions are subdivided into three cases according to Zhang and Anthes (1982) and the function  
 152 forms are given by Eqs. (13), (14), and (15).

153 (1) Strongly stable condition ( $Ri_B \geq 0.2$ ):

$$154 \quad \psi_M = \psi_H = -10 \ln \frac{z}{z_0}. \quad (13)$$

155 (2) Weakly stable condition ( $0 < Ri_B < 0.2$ ):

$$156 \quad \psi_M = \psi_H = -5 \left( \frac{Ri_B}{1.1 - 5Ri_B} \right) \ln \frac{z}{z_0}. \quad (14)$$

157 (3) Neutral condition ( $Ri_B = 0$ ):

$$158 \quad \psi_M = \psi_H = 0. \quad (15)$$

159 (4) Unstable condition ( $Ri_B < 0$ ):

$$160 \quad \psi_M = 2 \ln \frac{1+x}{2} + \ln \frac{1+x^2}{2} - 2 \arctan(x) + \frac{\pi}{2}, \quad (16a)$$

$$161 \quad \psi_H = 2 \ln \frac{1+y}{2}, \quad (16b)$$

162 where  $x = (1 - 16\zeta)^{1/4}$ ,  $y = (1 - 16\zeta)^{1/2}$ .

163 This scheme calculates turbulent fluxes of the momentum and sensible heat with  $u_*$  and  $\theta_*$ . In order to avoid the huge  
 164 difference of  $u_*$  through the two computations,  $u_*$  is arithmetically averaged with its previous value by Eq. (17), and a lower  
 165 limit of  $u_* = 0.1$  m/s is imposed to prevent the heat flux from being zero under very stable conditions. According to the  
 166 profile functions of wind and temperature near the ground,  $\theta_*$  then is deduced by Eq. (18).

$$167 \quad u_* = \frac{1}{2} \left( u_* + \frac{ku}{\ln \frac{z}{z_{0m}} - \psi_M} \right), \quad (17)$$

$$168 \quad \theta_* = \frac{k(\theta - \theta_g)}{R[\ln \frac{z}{z_{0h}} - \psi_H]}. \quad (18)$$

169 The calculation procedure of the Li scheme is the following: (1) determine  $Ri_B$ ,  $z_{0m}$  and  $z_{0h}$  according to the  
 170 observation data; (2) calculate  $\zeta$  with  $Ri_B$ ,  $z_{0m}$  and  $z_{0h}$ ; (3) calculate the momentum and sensible heat fluxes under different  
 171 conditions. The MM5 scheme is summarized as follows: (1) determine the universal functions according to the values of  $Ri_B$   
 172 and  $z_0$ ; (2) calculate the  $u_*$  and  $\theta_*$  with the meteorological variables and flux data; (3) derive the turbulent fluxes. Compared  
 173 with other non-iterative schemes including MM5, the Li scheme can be applied to the full range of roughness status  $10 \leq$   
 174  $\frac{z}{z_{0m}} \leq 10^5$  and  $-0.5 \leq \ln \frac{z_{0m}}{z_{0h}} \leq 30$  under whole conditions  $-5 \leq Ri_B \leq 2.5$ . In addition, there are three obvious differences  
 175 between the Li and MM5 schemes: (1) Li distinguishes  $z_{0h}$  from  $z_{0m}$  but MM5 does not distinguish them; (2) the two  
 176 schemes apply different universal functions under stable condition; (3) Li considers the RSL effect while MM5 ignores it.

### 177 3 Observational data and methods

178 The observational fluxes used in this study were measured at Gucheng station from December 1, 2016 to January 9, 2017.  
179 Gucheng station (115.40 ° E, 39.08 ° N) is located at Gucheng County, Baoding, Hebei province and it is about 110km  
180 southwest of Beijing (Fig. 1a). This station has a farmland site where rice is planted in summer and wheat in winter. The  
181 surroundings are mainly farmland and scattered villages (Fig. 1b). At Gucheng station, the momentum and sensible heat fluxes  
182 near the surface were measured by the eddy correlation flux measurement system. The system is mainly composed of a sonic  
183 anemometer (CSAT3) and a gas analyzer (LI-7500). They are set up at 4 m height above the surface ground. The measured  
184 fluxes are used to evaluate the two schemes as well as estimate the roughness lengths. The measured meteorological variables  
185 including wind speed and direction, temperature, humidity, pressure, radiation are utilized to calculate the momentum and  
186 sensible heat fluxes both in the Li and MM5 schemes. Note the observed meteorological data were from Gucheng station and  
187 national basic automatic weather stations in Jing-Jin-Ji in east China, respectively. Hourly surface PM<sub>2.5</sub> mass concentration  
188 in Baoding and Beijing from China National Environmental Monitoring Centre (<http://www.cnemc.cn/>) was also used in this  
189 paper.

#### 190 3.1 Data processing

191 To obtain accurate flux data, quality control has been performed for the observational data, including: (1) eliminate the  
192 outliers and the data in rainy days; (2) double rotation and WPL correction (Webb et al., 1980); (3) omit the dataset when the  
193 wind speed is less than 0.5 m s<sup>-1</sup>. In addition, the wind field especially the wind direction has a great impact on the value of  
194  $z_{0m}$ , so it is necessary to understand the situation at Gucheng station. Figure 2 shows the distribution frequency of wind speed  
195 and wind direction at Gucheng during the observation (December 1, 2016 ~ January 9, 2017). The wind speed is stable during  
196 this period and the maximum is no more than 5 m s<sup>-1</sup> and most of them are about 1 ~ 2 m s<sup>-1</sup>. The wind direction is relatively  
197 uniform except for the southeast wind (135 °).

#### 198 3.2 Determination of surface skin temperature

199 The surface skin temperature at Gucheng station is calculated from the radiation data by the following formula:

$$200 R_{lw}^{\uparrow} = (1 - \varepsilon_s)R_{lw}^{\downarrow} + \varepsilon_s\sigma T_g^4, \quad (19)$$

201 where  $R_{lw}^{\uparrow}$  and  $R_{lw}^{\downarrow}$  are the surface upward longwave radiation and long wave radiation incident on the surface,  
202 respectively.  $\sigma$  is the Stephen Boltzmann constant,  $\sigma = 5.67 \times 10^{-8} \text{ W m}^{-2} \text{ K}^{-4}$ .  $T_g$  is the surface skin temperature,  $\varepsilon_s$  is  
203 the surface emissivity which is the prerequisite for calculating  $T_g$ . Many researches estimated  $\varepsilon_s$  and the range of the values  
204 is always 0.9 ~ 1 (Stewart et al., 1994; Verhoef et al., 1997). According to the semi-empirical method in Yang et al. (2008),  $\varepsilon_s$   
205 is estimated when the RMSE is minimal. In this paper, the Li and MM5 schemes were used to estimate the  $\varepsilon_s$  value (as shown

206 in Fig. 3). It is clear that the  $\varepsilon_s$  value corresponding to the minimum RMSE is not very sensitive to the choice of two schemes.  
 207 When  $\varepsilon_s$  is 1, the RMSE has the minimum value. Thus, this experiment takes 1 as the optimal value of  $\varepsilon_s$ .

### 208 3.3 Determination of roughness length $z_{0m}$ ( $z_{0h}$ )

209 Using the observed momentum and sensible heat fluxes and the meteorological variables including wind speed,  
 210 temperature, humidity and pressure after quality control at Gucheng station,  $z_{0m}$  and  $z_{0h}$  were derived from Eqs. (20a) and  
 211 (20b) following Yang et al. (2003) and Sicart et al. (2014).

$$212 \frac{u_*}{u} = \frac{k}{\ln \frac{z}{z_{0m}} - \psi_M}, \quad (20a)$$

$$213 \frac{\theta_*}{(\theta - \theta_g)} = \frac{k}{R [\ln \frac{z}{z_{0h}} - \psi_H]}. \quad (20b)$$

214 During the observation period, the crops stopped growing and the height did not exceed 0.1 m, so the zero-plane  
 215 displacement height was ignored hence the reference height  $z$  was taken as 4m. The observation time was too short (about 1  
 216 month) to consider the effect of seasonal variations on roughness lengths. Thus,  $z_{0m}$  and  $z_{0h}$  were assumed as two fixed  
 217 values. Based on the variables and formulae mentioned above, the roughness lengths at Gucheng are derived:  $z_{0m} =$   
 218 0.0419 m,  $z_{0h} = 0.0042$  m.

## 219 4 Results and discussion

220 The RSL, roughness length and their influence on the calculation of turbulent flux are discussed in detail in this section.  
 221 The Li and MM5 schemes are offline tested and evaluated during the haze pollution from December 13 to 23, 2016.

### 222 4.1 The influence of RSL and roughness length on the calculation of turbulent flux

223 The RSL is usually defined as the region where the flow is influenced by the individual roughness elements as reflected  
 224 by the spatial inhomogeneity of the mean flow (Florens et al., 2013). In the RSL, turbulence is strongly affected by individual  
 225 roughness elements, and the standard MOST is no longer valid (Simpson et al., 1998). Therefore, it is necessary to consider  
 226 the RSL effect in the calculation of turbulent flux, especially for the rough terrain such as forest or large cities.  $z_{0m}$  is defined  
 227 as the height at which the extrapolated wind speed following the similarity theory vanishes. It is mainly determined by land-  
 228 cover type and canopy height after excluding large obstructions. In models,  $z_{0m}$  is always based on the look-up table which  
 229 is related to land-cover types. In this study,  $z_{0m}$  was simply classified based on the research of Stull (1988) listed in Table 1.  
 230 It can be seen in Table 1 that the rougher underlying surface corresponds to the larger value of  $z_{0m}$ .  $z_{0h}$  is the height at which  
 231 the extrapolated air temperature is identical to the surface skin temperature. Some early researchers assumed that  $z_{0m}$  was  
 232 equal to  $z_{0h}$  (Louis, 1979; Louis et al., 1982). However, the assumption is not applicable in reality because  $z_{0m}$  and  $z_{0h}$   
 233 have different physical meanings. Different treatment of  $z_{0m}$  and  $z_{0h}$  may introduce considerable changes in the surface



234 flux calculation (Launiainen, 1995; Kot and Song, 1998; Anurose and Subrahmanyam, 2013). Many studies removed the  
 235 assumption that  $z_{0m}$  was equal to  $z_{0h}$  and made the schemes more applicable in the situation that  $z_{0m}$  was not equal to  $z_{0h}$   
 236 or the ratio of  $z_{0m}$  to  $z_{0h}$  was much large (Wouters et al., 2012; Li et al., 2014; Li et al., 2015). Some field experiments even  
 237 indicated the ratio  $z_{0m}/z_{0h}$  has a diurnal variation (Sun, 1999; Yang, 2003; Yang, 2008). In this study, we make the common  
 238 assumption that the ratio  $z_{0m}/z_{0h}$  is a constant.

239 Considering the lowest level in mesoscale models is usually about 10m,  $z = 10$  m is set as the reference height. The  
 240 range of  $Ri_B$  is set according to Louis82 (Louis et al., 1982) in the following discussion. Firstly, the effects of different land-  
 241 cover types (different  $z_{0m}$  values) and RSL on flux calculation were discussed. Set  $z_{0m} = z_{0h}$ , corresponding to four  
 242 cases:  $z_{0m} = 1, 0.5, 0.05, 0.001$  m. These cases correspond to large cities, forests, agricultural fields and wide water surface,  
 243 respectively. Figure 4 shows the relationship between  $C_M(C_H)$  and  $Ri_B$  for different  $z_{0m}$  values and treatment of RSL. It  
 244 can be seen that both RSL and  $z_{0m}$  have impacts on  $C_M$  and  $C_H$ . Ignoring the RSL effect results in larger  $C_M$  and  $C_H$ ,  
 245 compared with the results of original scheme considering the RSL. The difference induced by RSL is evident only under the  
 246 rough surface. For example, the difference under  $z_{0m} = 1$  is obviously greater than other  $z_{0m}$  settings, and when  $z_{0m}$  is  
 247 reduced to 0.05 or less, the RSL has little effect. Furthermore, the RSL contributes more to sensible heat transfer than to  
 248 momentum transfer under the same setting of  $z_{0m}$ . The effects of different land-cover types on  $C_M$  and  $C_H$  are much more  
 249 significant compared with RSL. The rougher the surface is (corresponding to the larger  $z_{0m}$  value), the larger the  $C_M$  ( $C_H$ )  
 250 is. In addition, there is a corresponding relationship between  $C_M(C_H)$  and stability. The more unstable the atmosphere is, the  
 251 larger difference the value of  $C_M(C_H)$  is and vice versa. Once  $Ri_B$  exceeds the critical value (generally  $0.2 \sim 0.25$ ), the  
 252 transfer coefficients decline sharply but still above 0.

253 Secondly, the effects of difference between  $z_{0m}$  and  $z_{0h}$  as well as RSL on flux calculation are discussed. The  
 254 relationship between  $z_{0m}$  and  $z_{0h}$  can be expressed as  $kB^{-1} = \ln \frac{z_{0m}}{z_{0h}}$ . Over the sea,  $z_{0m}$  is comparable to  $z_{0h}$ ; over the  
 255 uniform vegetation surface (grassland, farmland, woodland),  $kB^{-1}$  is about 2 ( $z_{0m}/z_{0h} \approx 10$ ) (Garratt and Hicks, 1973;  
 256 Garratt, 1978; Garratt and Francey, 1978), which coincides with our results in Gucheng ( $z_{0m} = 0.0419$  m,  $z_{0h} = 0.0042$  m);  
 257 over the surface with bluff roughness elements, the  $kB^{-1}$  value may be very large. For example, in some large cities,  $kB^{-1}$   
 258 is even up to 30 ( $z_{0m}/z_{0h} \approx 10^{13}$ ) (Sugawara and Narita, 2009). Therefore, the ratio  $z_{0m}/z_{0h}$  varies over a wide range.  
 259 Figure 5 shows the relationship between  $C_M(C_H)$  and  $Ri_B$  for different treatment of  $z_{0m}/z_{0h}$ . Set  $z_{0m} = 1$  as a large city  
 260 case,  $z_{0h} = 1, 0.01, 10^{-4}, 10^{-6}$  m, and the large differences derived from the different ratios are displayed in Fig. 5. The similar  
 261 RSL effect can be found compared with Fig. 4. The differences induced by RSL are more obvious than that in Fig. 4. The  
 262 different treatment of ratio  $z_{0m}/z_{0h}$  has great impact on turbulent flux transfer, particularly for sensible heat transfer. It seems  
 263 evident that when  $z_{0h}$  is not equal to  $z_{0m}$  ( $z_{0m}/z_{0h} = 100 \sim 10^6$ ), the calculated  $C_H$  is much small compared to the treatment

264 that  $z_{0h}$  is equal to  $z_{0m}$  ( $z_{0m}/z_{0h}=1$ ). In addition,  $C_M(C_H)$  decreases with the increase of stability, and they decrease much  
265 slower when  $z_{0h}$  is not equal to  $z_{0m}$ .

266

#### 267 **4.2 Comparison of momentum and sensible heat fluxes calculated by the two schemes**

268 Using the obtained roughness lengths and the observations, the momentum and sensible heat flux were calculated by the  
269 Li and MM5 schemes. Firstly,  $z_{0m}$  and  $z_{0h}$  were set as 0.0419 and 0.0042 respectively in the Li scheme,  $z_0$  was equal to  
270  $z_{0m}$  in the MM5 scheme to calculate the momentum and sensible heat fluxes and the results are shown in Figs. 6a and 6b. It  
271 can be seen that compared with MM5, Li performs better with higher regression coefficient and determination coefficient. For  
272 the momentum fluxes, the regression coefficient by Li is 0.6795 and that by MM5 is 0.5598, indicating that the error of Li is  
273 12 % lower than that of MM5. For sensible heat fluxes, the regression coefficient by Li is 0.7967 and that by MM5 is 1.7994.  
274 The latter is much larger than 1, that is, the MM5 scheme obviously overestimates the sensible heat due to it does not distinguish  
275  $z_{0h}$  from  $z_{0m}$ . Then, make  $z_0$  equal to 0.0042 in the MM5 scheme to re-calculate the sensible heat fluxes as shown in Fig.  
276 6c. It can be seen the result has a great improvement after modifying  $z_0$  value and the regression coefficient by MM5 is  
277 0.7363, indicating that the error was reduced by 54 % after considering the  $z_{0h}$  effect. The result indicates that  $z_{0h}$  plays a  
278 critical role in both the SL scheme and the sensible heat flux (Chen and Zhang, 2009; Chen et al., 2011). However, the error  
279 caused by Li is still 6 % lower than that by MM5. This illustrates that in addition to the effect of roughness lengths, the  
280 algorithm of the Li scheme itself is more reasonable than that of MM5 scheme.

#### 281 **4.3 The specific performance of the two schemes in the severe haze pollution**

282 There were two obvious pollution processes during this observation period and one occurred during December 13 to 23,  
283 2016. Figure 7 shows the variations of hourly observed  $PM_{2.5}$  concentration as well as the momentum and sensible heat fluxes  
284 calculated by the Li and MM5 schemes at Gucheng station in this process. For the research purpose significance, only the  
285 daytime (from 8:00 a.m. to 20:00 p.m.) was taken into account. Note in MM5,  $z_0$  was 0.0419 when calculate momentum  
286 fluxes and it was 0.0042 when calculate sensible heat fluxes. As shown in Fig. 7, the calculated results of momentum and  
287 sensible heat fluxes for the two schemes are generally consistent with the trend of the observations. Specifically, for the  
288 momentum fluxes (Fig. 7a), the results of two schemes have little difference when the values of observed momentum fluxes  
289 are large or at the peak. When the observed momentum fluxes are small, the Li scheme results are close to or less than the  
290 observations, while the MM5 scheme results are always higher than observations because of the limit of  $u_* = 0.1$  in this  
291 scheme. For the sensible heat fluxes (Fig. 7b), MM5 results are always lower while Li results are closer to observations  
292 especially when the observed values are small. Furthermore, according to the evolution of  $PM_{2.5}$  concentration, this haze event  
293 was then divided into three stages: the clear stage (stage 1: 13~14), the transition stage (stage 2: 16~18) and the maintenance

294 stage (stage 3: 21~22). As shown in Fig. 7, in the clear stage (stage 1), the atmospheric stratification is unstable,  $PM_{2.5}$   
295 concentration is low and there is a strong flux transport in the SL, the corresponding observations of the momentum and  
296 sensible heat fluxes are relatively high and they vary greatly. In the transition stage (stage 2), the atmosphere is changing from  
297 unstable to stable corresponding to haze formation, the momentum and sensible heat fluxes gradually decreases and the daily  
298 variation also decreases. In the maintenance stage (stage 3), the atmospheric stratification is very stable, and flux transport in  
299 the SL is weak, both the momentum and sensible heat fluxes are at a low level. It can be seen that the Li results are generally  
300 closer to the observations compared with MM5 results in all three stages.

301 Figure 8 shows the probability distribution functions (PDF) of the difference of momentum fluxes (Figs. 8a, 8c, 8e, 8g)  
302 and sensible heat fluxes (Figs. 8b, 8d, 8f, 8h) calculated by using the Li and MM5 schemes in different stages at Gucheng  
303 station. In the whole pollution process, for the momentum fluxes (Fig. 8a), the PDF of the difference by Li tends to cluster in  
304 a narrower range centered by 0, and the probability within  $\pm 0.005 N m^{-2}$  is 46.82 %, while this value by MM5 falls to 23.02 %.  
305 For the sensible heat fluxes (Fig. 8b), the PDF of the difference by Li is also more concentrated around 0 than that by MM5.  
306 The probabilities of bias by Li and MM5 within  $\pm 2.5 W m^{-2}$  are 32.54 % and 13.49 %, respectively. In stage 1, for the  
307 momentum fluxes (Fig. 8c), the probability of bias by Li within  $\pm 0.005 N m^{-2}$  is 38.09 %. The bias of MM5 mainly concentrates  
308 larger than 0, and the probability within  $\pm 0.005 N m^{-2}$  is 14.29 %. For the sensible heat fluxes (Fig. 8d), the probability of Li  
309 bias within  $\pm 2.5 W m^{-2}$  is 38.09 %, the same as momentum fluxes. The bias of MM5 mainly concentrates less than 0, and the  
310 probability within  $\pm 2.5 W m^{-2}$  is 9.52 %. In stage 2, the differences between the two schemes are more obvious. The momentum  
311 and sensible heat fluxes bias by Li is the most concentrated around 0 in all cases, while the distribution of bias by MM5 is  
312 similar to that in stage 1. Specifically, for the momentum fluxes (Fig. 8e), the probabilities of bias by Li and MM5 within  
313  $\pm 0.005 N m^{-2}$  are 56.25 % and 25.00 %. For the sensible heat fluxes (Fig. 8f), the probabilities of bias by Li and MM5 within  
314  $\pm 2.5 W m^{-2}$  are 40.62 % and 6.25 %. In stage 3, the difference between two schemes is small. For the momentum fluxes (Fig.  
315 8g), the probabilities of bias by Li and MM5 within  $\pm 0.005 N m^{-2}$  are 22.73 % and 27.27 %. For the sensible heat fluxes (Fig.  
316 8h), the probabilities of bias by Li and MM5 within  $\pm 2.5 W m^{-2}$  are both 36.36 %.

317 Mean bias (MB), normalized mean bias (NMB), normalized mean error (NME) and root mean square error (RMES) of  
318 Li and MM5 were calculated to test the two schemes. Table 2 shows that the Li scheme generally estimates better than the  
319 MM5 scheme. In the whole haze process, the Li scheme underestimates the momentum fluxes by 3.63 % relative to the  
320 observations, while the MM5 scheme overestimates by 34.03 %. The Li and MM5 schemes underestimate the sensible heat  
321 fluxes by 15.69 % and 50.22 %, respectively. In the three stages, the Li scheme performs much better than the MM5 scheme  
322 in the stage 1 and stage 2, especially in stage 2 when atmospheric stratification transforms from unstable to stable condition,  
323 the difference between the Li and MM5 schemes are particularly significant. The Li and MM5 schemes overestimate the  
324 momentum fluxes by 7.68% and 45.56 %, respectively, while Li and MM5 underestimate the sensible heat fluxes by 33.84 %

325 and 76.88 %. The error of Li is much less than that of MM5. Considering the importance of atmospheric stratification in the  
326 generation and accumulation of PM<sub>2.5</sub> in stage 2, the Li scheme is expected to show better performance in online simulation of  
327 PM<sub>2.5</sub> than MM5.

328 Based on the good behavior of the Li scheme in Gucheng, the same experiment was performed at Beijing station to discuss  
329 the effect of different land-cover types on flux calculation for two schemes. For Beijing station, the assumption  $z_{0m} = 1$  m,  
330  $z_{0m}/z_{0h} = 10^6$  was made to represent the surface condition of megacity due to a lack in situ measurements of surface  
331 turbulent flux. As shown in Fig. 9, the evolution of PM<sub>2.5</sub> concentration at Beijing station was also divided into three stages  
332 (stage 1: 13~15; stage 2: 17~19; stage 3: 20~21) just like Gucheng in the discussion. Compare to Fig. 7, there is a significant  
333 increase in the difference of momentum and sensible heat fluxes between Li and MM5 in Fig. 9. To be specific, the momentum  
334 transfer in Beijing is obviously larger than that in Gucheng due to the great increase of the urban aerodynamic roughness length  
335 ( $z_{0m}$ ). In the meanwhile, the difference between Li and MM5 has a further expansion at Beijing station compared with Gucheng.  
336 The sensible heat transfer by the Li scheme has great difference between clear days and pollution days, which is, the sensible  
337 heat transfer changes acutely in the stage 1 while it changes smoothly in the stage 2 and stage 3. The sensible heat transfer by  
338 the MM5 scheme is significantly different compared with Li result due to MM5 ignored the  $z_{0m}$  effect, and the small number  
339 of  $z_{0h}$  keeps the sensible heat fluxes at a low level in all three stages.

340 To quantify the differences between the two schemes, a relative difference is defined in percentage:

$$341 \quad \Delta V = \left| \frac{V_{Li} - V_{MM5}}{V_{MM5}} \right| \times 100 \%, \quad (21)$$

342 where  $V_{Li}$  and  $V_{MM5}$  are the momentum (or sensible heat) flux calculated by the Li and MM5 schemes, respectively. We  
343 obtained the relative differences at the two stations in the three stages through the statistics. It is clearly that the largest relative  
344 difference at Gucheng station is in the stage 2 and the value at Beijing station is in the stage 1. The differences in Beijing are  
345 always larger than that in Gucheng for each three stages. Specifically, the relative difference of momentum flux in stage 1,  
346 stage 2 and stage 3 increases by 73 %, 34 % and 27 %, respectively, and the results of sensible heat flux are 289 %, 52 % and  
347 68 %, respectively.

348 We further tested the two schemes in whole Jing-Jin-Ji region. Figure 10 shows the mean momentum and sensible heat  
349 fluxes calculated by Li and MM5 schemes and their difference in Jing-Jin-Ji during the pollution episode. The assumption  
350  $z_{0m} = 0.1$  m,  $z_{0m}/z_{0h} = 10^3$  were used to represent the average condition of the underlying surface of Jing-Jin-Ji region.  
351 As shown in Fig. 10, the momentum fluxes calculated by Li are less than that by MM5 in most stations; the sensible heat fluxes  
352 calculated by Li are usually larger than that by MM5. The result is consistent with the experiment of Gucheng station, which  
353 further indicates the importance of considering  $z_{0m}$  and  $z_{0h}$  at the same time.

## 354 5 Conclusions

355 Using the observed momentum and sensible heat fluxes, together with conventional meteorological data including  
356 pressure, temperature, humidity and wind speed from December 1, 2016 to January 9, 2017, including a severe pollution  
357 episode from December 13 to 23, 2016, the differences and the performance of the two surface schemes were discussed and  
358 evaluated in this paper. The evolution process of atmospheric stratification from unstable to stable corresponding to  $PM_{2.5}$   
359 increasing was mainly discussed. The contributions of roughness lengths ( $z_{0m}$  and  $z_{0h}$ ) as well as other factors in the SL  
360 schemes to the momentum and sensible heat flux calculation were also discussed in details. The results are summarized as  
361 follows:

362 1)  $z_{0m}$  and  $z_{0h}$  have important effects on turbulent flux calculation in the SL schemes. Different values of  $z_{0m}$  and  
363  $z_{0h}$  in the schemes could induce great changes in the flux calculation, indicating that it is very necessary and important to  
364 distinguish  $z_{0h}$  from  $z_{0m}$ . Ignoring the difference between the two in the MM5 scheme led to large errors in the calculation  
365 of sensible heat fluxes and this error in Gucheng is 54 %. Besides the roughness lengths, the algorithms of two schemes are  
366 also one of the important factors. In addition, ignoring the effect of the RSL in schemes may also result in certain bias of  
367 momentum and sensible heat fluxes in megacity regions which represent the rough underlying surface.

368 2) The effect of  $z_{0m}/z_{0h}$  on turbulent fluxes is closely related to land-cover types ( $z_{0m}$ ). A rough land-cover type (large  
369  $z_{0m}$ ) should be accompanied by a large value of  $z_{0m}/z_{0h}$ . The differences of momentum and sensible heat fluxes calculated  
370 by Li and MM5 were much bigger in Beijing than that in Gucheng. This suggests that the MM5 scheme probably induces  
371 bigger error in megacities with rough surface (e.g., Beijing) than it in suburban area with smooth surface (e.g., Gucheng) due  
372 to the irrational algorithm of MM5 scheme itself and the ignoring difference between  $z_{0m}$  and  $z_{0h}$ .

373 3) The Li scheme generally performed better than the MM5 scheme in the calculation of both the momentum flux and  
374 the sensible heat flux compared with observations at Gucheng station. The Li scheme made a better description in atmospheric  
375 stratification which is closely related to the haze pollution, compared with the MM5 scheme. This advantage was the most  
376 prominent in the transition stage from unstable to stable atmospheric stratification corresponding to the  $PM_{2.5}$  accumulation.  
377 In this stage, the momentum flux calculated by Li was overestimated by 7.68 % and this overestimation by MM5 was up to  
378 45.56 %; the sensible heat flux by Li was underestimated by 33.84 % while this underestimation by MM5 was even up to  
379 76.88 %. In most Jing-Jin-Ji region, the momentum fluxes calculated by Li were less than that by MM5 and the sensible heat  
380 fluxes by Li were larger than that by MM5, which was consistent with Gucheng.

381 The offline study of the two SL schemes in this paper showed the superiority of the Li scheme for surface flux calculation  
382 corresponding to the  $PM_{2.5}$  evolution during the haze episode in Jing-Jin-Ji in east China. The study results offer the prerequisite  
383 and a possible way to improve PBL diffusion simulation and then  $PM_{2.5}$  prediction, which will be achieved in the follow-up  
384 work of online integrating of the Li scheme into the atmosphere chemical model.

385 **Acknowledgments**

386 The study was supported by the National Key Project (2016YFC0203306, 2016YFC0203304), the National (Key) Basic  
387 Research and Development (973) Program of China (2014CB441201), the National Natural Science Foundation of China  
388 (41505004, 41675009), and Jiangsu Provincial Natural Science Fund Project (BK20150910).

389 **References**

- 390 Anurose, T. J., and Subrahmanyam, D. B.: Improvements in Sensible Heat-Flux Parametrization in the High-Resolution  
391 Regional Model (HRM) Through the Modified Treatment of the Roughness Length for Heat, *Bound.-Lay. Meteorol.*,  
392 147, 569-578, <https://doi.org/10.1007/s10546-013-9799-9>, 2013.
- 393 Ban, J., Gao, Z., and Lenschow, D. H.: Climate simulations with a new air-sea turbulent flux parameterization in the  
394 National Center for Atmospheric Research Community Atmosphere Model (CAM3), *J. Geophys. Res.-Atmos.*, 115,  
395 <https://doi.org/10.1029/2009JD012802>, 2010.
- 396 Beljaars, A. C. M., and Holtslag, A. A. M.: Flux parameterization over land surfaces for atmospheric models, *J. Appl.*  
397 *Meteor.*, 30, 327-341, 1991.
- 398 Businger, J. A., Wyngaard, J. C., Izumi, Y., and Bradley, E. F.: Flux-profile relationships in the atmospheric surface layer, *J.*  
399 *Atmos. Sci.*, 28, 181-189, 1971.
- 400 Businger, J. A.: Transfer of momentum and heat in the planetary boundary layer, *Proc. Symp. Arctic Heat Budget and*  
401 *Atmospheric Circulation*, RM-5233-NSF, 305-331, 1966.
- 402 Chen, F., and Zhang, Y.: On the coupling strength between the land surface and the atmosphere: From viewpoint of surface  
403 exchange coefficients, *Geophys. Res. Lett.*, 36, <https://doi.org/10.1029/2009GL037980>, 2009.
- 404 Chen, Y., Yang, K., He, J., Qin, J., Shi, J., Du, J., and He, Q.: Improving land surface temperature modeling for dry land of  
405 China, *J. Geophys. Res.-Atmos.*, 116, <https://doi.org/10.1029/2011JD015921>, 2011.
- 406 Cheng, F. Y., Chin, S. C., and Liu, T. H.: The role of boundary layer schemes in meteorological and air quality simulations of  
407 the Taiwan area, *Atmos. Environ.*, 54, 714-727, <https://doi.org/10.1016/j.atmosenv.2012.01.029>, 2012.
- 408 Cheng, Y., and Brutsaert, W.: Flux-profile relationships for wind speed and temperature in the stable atmospheric boundary  
409 layer, *Bound.-Lay. Meteorol.*, 114, 519-538, <https://doi.org/10.1007/s10546-004-1425-4>, 2005.
- 410 De Ridder, K.: Bulk Transfer Relations for the Roughness Sublayer, *Bound.-Lay. Meteorol.*, 134, 257-267,  
411 <https://doi.org/10.1007/s10546-009-9450-y>, 2010.
- 412 Dyer, A. J.: A review of flux-profile relationships, *Bound.-Lay. Meteorol.*, 7, 363-372, <https://doi.org/10.1007/BF00240838>,  
413 1974.

414 Dyer, A. J.: The turbulent transport of heat and water vapour in an unstable atmosphere, *Quart. J. Roy. Meteor. Soc.*, 93, 501-  
415 508, <https://doi.org/10.1002/qj.49709339809>, 1967.

416 Florens, E., Eiff, O., and Moulin, F.: Defining the roughness sublayer and its turbulence statistics, *Exp. Fluids*, 54, 1500,  
417 <https://doi.org/10.1007/s00348-013-1500-z>, 2013.

418 Garratt, J. R., and Francey, R. J.: Bulk characteristics of heat transfer in the unstable, baroclinic atmospheric boundary layer,  
419 *Bound.-Lay. Meteorol.*, 15, 399-421, <https://doi.org/10.1007/BF00120603>, 1978.

420 Garratt, J. R., and Hicks, B. B.: Momentum, heat and water vapour transfer to and from natural and artificial surfaces, *Quart.*  
421 *J. Roy. Meteor. Soc*, 99, 680-687, 1973.

422 Garratt, J. R.: Transfer characteristics for a heterogeneous surface of large aerodynamic roughness, *Quart. J. Roy. Meteor.*  
423 *Soc.*, 104, 491-502, 1978.

424 Högström, U.: Review of some basic characteristics of the atmospheric surface layer, *Bound.-Lay. Meteorol.*, 78, 215-246,  
425 <https://doi.org/10.1007/BF00120937>, 1996.

426 Holtslag, A. A. M., and De Bruin, H. A. R.: Applied modeling of the nighttime surface energy balance over land, *J. Appl.*  
427 *Meteor.*, 27, 689-704, 1988.

428 Hu, X. M., Nielsen-Gammon, J. W., and Zhang, F.: Evaluation of three planetary boundary layer schemes in the WRF model,  
429 *J. Appl. Meteorol. Climatol*, 49, 1831-1844, <https://doi.org/10.1175/2010JAMC2432.1>, 2010.

430 Jiménez, P. A., Dudhia, J., González-Rouco, J. F., Navarro, J., Montávez, J. P., and García-Bustamante, E.: A revised scheme  
431 for the WRF surface layer formulation, *Mon. Wea. Rev.*, 140, 898-918, <https://doi.org/10.1175/MWR-D-11-00056.1>,  
432 2012.

433 Kot, S. C., and Song, Y.: An Improvement of the Louis Scheme for the Surface Layer in an Atmospheric Modelling System,  
434 *Bound.-Lay. Meteorol.*, 88, 239-254, <https://doi.org/10.1023/A:1001119329423>, 1998.

435 Launiainen, J.: Derivation of the relationship between the Obukhov stability parameter and the bulk Richardson number for  
436 flux-profile studie, *Bound.-Lay. Meteorol.*, 76, 165-179, <https://doi.org/10.1007/BF00710895>, 1995.

437 Li, T., Wang, H., Zhao, T., Xue, M., Wang, Y., Che, H., and Jiang, C.: The Impacts of Different PBL Schemes on the  
438 Simulation of PM<sub>2.5</sub> during Severe Haze Episodes in the Jing-Jin-Ji Region and Its Surroundings in China, *Adu.*  
439 *Meteorol.*, <http://dx.doi.org/10.1155/2016/6295878>, 2016a.

440 Li, Y., Gao, Z., Li, D., Chen, F., Yang, Y., and Sun, L.: An Update of Non-iterative Solutions for Surface Fluxes Under  
441 Unstable Conditions, *Bound.-lay. Meteorol.*, 156, 501-511, <https://doi.org/10.1007/s10546-015-0032-x>, 2015.

442 Li, Y., Gao, Z., Li, D., Chen, F., Yang, Y., and Sun, L.: Erratum to: An Update of Non-iterative Solutions for Surface Fluxes  
443 Under Unstable Conditions, *Bound.-Lay. Meteorol.*, 161: 225-228, 2016b.

444 Li, Y., Gao, Z., Li, D., Wang, L., and Wang, H.: An improved non-iterative surface layer flux scheme for atmospheric stable  
445 stratification conditions, *Geosci. Model Dev.*, 7, 515-529, <https://doi.org/10.5194/gmd-7-515-2014>, 2014.

446 Li, Y.: *On the Surface Turbulent Fluxes Calculation in Numerical Models*, Beijing: university of Chinese academy of  
447 sciences, 2014.

448 Li, Z., Guo, J., Ding, A., Liao, H., Liu, J., Sun, Y., Wang, T., Xue, H., Zhang, H., and Zhu, B.: Aerosol and boundary-layer  
449 interactions and impact on air quality, *Natl. Sci. Rev.*, 4, 810–833, <https://doi.org/10.1093/nsr/nwx117>, 2017.

450 Liu, T. T., Gong, S. L., He, J. J., Yu, M., Wang, Q. F., Li, H. R., Liu, W., Zhang, J., Li, L., Wang, X. G., Li, S. L., Lu, Y. L.,  
451 Du, H. T., Wang, Y. Q., Zhou, C. H., Liu, H. L. and Zhao, Q. C.: Attributions of meteorological and emission factors to  
452 the 2015 winter severe haze pollution episodes in China's Jing-Jin-Ji area, *Atmos. Chem. Phys.*, 17, 2971–2980,  
453 <https://doi.org/10.5194/acp-17-2971-2017>, 2017.

454 Louis, J. F.: A parametric model of vertical eddy fluxes in the atmosphere. *Bound.-Lay. Meteorol.*, 17, 187-202,  
455 <https://doi.org/10.1007/BF00117978>, 1979.

456 Louis, J. F., Tiedtke, M., and Geleyn, J. F.: A short history of the operational PBL parameterization at ECMWF, in *Workshop*  
457 *on Planetary Boundary Layer Parameterization*, November 1981, ECMWF, Reading, U.K., pp. 59–79, 1982.

458 Monin, A. S., and Obukhov, A. M.: Basic laws of turbulent mixing in the surface layer of the atmosphere, *Contrib. Geophys.*  
459 *Inst. Acad. Sci., USSR*, 24, 163–187, 1954.

460 Paulson, C. A.: The mathematical representation of wind speed and temperature profiles in the unstable atmospheric surface  
461 layer, *J. Appl. Meteorol.*, 9, 857-861, 1970.

462 Sharan, M., and Srivastava, P.; A Semi-Analytical Approach for Parametrization of the Obukhov Stability Parameter in the  
463 Unstable Atmospheric Surface Layer, *Bound.-Lay. Meteorol.*, 153, 339-353, [https://doi.org/10.1007/s10546-014-9948-](https://doi.org/10.1007/s10546-014-9948-9)  
464 [9](https://doi.org/10.1007/s10546-014-9948-9), 2014.

465 Sicart, J. E., Litt, M., Helgason, W., Tahar, V. B., and Chaperon, T.: A study of the atmospheric surface layer and roughness  
466 lengths on the high-altitude tropical Zongo glacier, Bolivia, *J. Geophys. Res.-Atmos.*, 119, 3793–3808,  
467 <https://doi.org/10.1002/2013JD020615>, 2014.

468 Simpson, I. J., Thurtell, G. W., Neumann, H. H., Den Hartog, G., and Edwards, G. C.: The Validity of Similarity Theory in  
469 the Roughness Sublayer Above Forests, *Bound.-Lay. Meteorol.*, 87, 69-99, <https://doi.org/10.1023/A:1000809902980>,  
470 1998.

471 Stewart, J. B., Kustas, W. P., Humes, K. S., Nichols, W. D., Moran, M. S., and De Bruin, H. A. R.: Sensible heat flux-  
472 radiometric surface temperature relationship for eight semiarid areas, *J. Appl. Meteorol.*, 33, 1110-1117, 1994.

473 Stull, R. B.: *An Introduction to Boundary Layer Meteorology*, Kluwer Academic Publishers, London, 1988.



474 Sugawara, H., and Narita, K.: Roughness length for heat over an urban canopy, *Theor. Appl. Climatol.*, 95, 291-299,  
475 <https://doi.org/10.1007/s00704-008-0007-7>, 2009.

476 Sun, J.: Diurnal Variations of Thermal Roughness Height over a Grassland, *Bound.-Lay. Meteorol.*, 92, 407-427,  
477 <https://doi.org/10.1023/A:1002071421362>, 1999.

478 Tymvios, F., Charalambous, D., Michaelides, S., and Lelieveld, J.: Intercomparison of boundary layer parameterizations for  
479 summer conditions in the eastern Mediterranean island of Cyprus using the WRF-ARW model, *Atmos. Res.*, 208, 45-  
480 59, <https://doi.org/10.1016/j.atmosres.2017.09.011>, 2017.

481 Vautard, R., Moran, M. D., Solazzo, E., Gilliam, R. C., Matthias, V., Bianconi, R., Chemel, C., Ferreira, J., Geyer, B.,  
482 Hansen, A. B., Jericevic, A., Prank, M., Segers, A., Silver, J. D., Werhahn, J., Eolke, R., Rao, S. T., and Galmarini, S.:  
483 Evaluation of the meteorological forcing used for the Air Quality Model Evaluation International Initiative (AQMEII)  
484 air quality simulations, *Atmos. Environ.*, 53, 15-37, <https://doi.org/10.1016/j.atmosenv.2011.10.065>, 2012.

485 Verhoef, A., De Bruin, H. A. R., and Van Den Hurk, B. J. J. M.: Some Practical Notes on the Parameter kB-1 for Sparse  
486 Vegetation., *J. Appl. Meteorol.*, 36, 560-572, 1997.

487 Wang, H., Shi, G. Y., Zhang, X. Y., Gong, S. L., Tan, S. C., Chen, B., Che, H. Z., and Li, T.: Mesoscale modeling study of the  
488 interactions between aerosols and PBL meteorology during a haze episode in China Jing-Jin-Ji and its near surrounding  
489 region - Part 2: Aerosols' radiative feedback effects, *Atmos. Chem. Phys.*, 15, 3277-3287, [https://doi.org/10.5194/acp-](https://doi.org/10.5194/acp-15-3277-2015)  
490 [15-3277-2015](https://doi.org/10.5194/acp-15-3277-2015), 2015b.

491 Wang, H., Tan, S. C., Wang, Y., Jiang, C., Shi, G., Zhang, M., and Che, H. Z.: A multisource observation study of the severe  
492 prolonged regional haze episode over eastern China in January 2013, *Atmos. Environ.*, 89, 807-815,  
493 <https://doi.org/10.1016/j.atmosenv.2014.03.004>, 2014.

494 Wang, H., Xue, M., Zhang, X. Y., Liu, H. L., Zhou, C. H., Tan, S. C., Che, H. Z., Chen, B., and Li, T.: Mesoscale modeling  
495 study of the interactions between aerosols and PBL meteorology during a haze episode in China Jing-Jin-Ji and its  
496 nearby surrounding region - Part 1: Aerosol distributions and meteorological features, *Atmos. Chem. Phys.*, 15, 3257-  
497 3275, <https://doi.org/10.5194/acp-15-3257-2015>, 2015a.

498 Wang, S., Wang, Q., and Doyle, J.: Some improvements to Louis surface flux parameterization. Paper presented at 15th  
499 symposium on boundary layers and turbulence, American Meteorological Society, 15-19, 2002, Wageningen,  
500 Netherlands.

501 Webb, E. K., Pearman, G. I., and Leuning, R.: Correction of flux measurements for density effects due to heat and water  
502 vapour transfer, *Quart. J. Roy. Meteor. Soc.*, 106, 85-100, 1980.

503 Webb, E. K.: Profile relationships: The log-linear range, and extension to strong stability, *Quart. J. Roy. Meteor. Soc.*, 96, 67-  
504 90, 1970.

505 Wouters, H., De Ridder, K., and van Lipzig, N. P. M.: Comprehensive Parametrization of Surface-Layer Transfer  
506 Coefficients for Use in Atmospheric Numerical Models, *Bound.-Lay. Meteorol.*, 145, 539-550,  
507 <https://doi.org/10.1007/s10546-012-9744-3>, 2012.

508 Xie, B., Fung, J. C. H., Chan, A., and Lau, A.: Evaluation of nonlocal and local planetary boundary layer schemes in the  
509 WRF model, *J. Geophys. Res.-Atmos.*, 117, 48-50, <https://doi.org/10.1029/2011JD017080>, 2012.

510 Yang, K., Koike, T., and Yang, D.: Surface Flux Parameterization in the Tibetan Plateau, *Bound.-Lay. Meteorol.*, 106, 245-  
511 262, <https://doi.org/10.1023/A:1021152407334>, 2003.

512 Yang, K., Koike, T., Ishikawa, H., Kim, J., Li, X., Liu, H., Liu, S., Ma, Y., and Wang, J.: Turbulent Flux Transfer over Bare-  
513 Soil Surfaces: Characteristics and Parameterization, *J. Appl. Meteorol. Clim.*, 47, 276-290,  
514 <https://doi.org/10.1175/2007jamc1547.1>, 2008.

515 Yang, K., Tamai, N., and Koike, T.: Analytical Solution of Surface Layer Similarity Equations, *J. Appl. Meteorol.*, 40, 1647-  
516 1653, 2001.

517 Yang, Y., Liu, X., Qu, Y., Wang, J., An, J., Zhang, Y., and Zhang, F.: Formation mechanism of continuous extreme haze  
518 episodes in the megacity Beijing, China, in January 2013, *Atmos. Res.*, 155, 192–203,  
519 <https://doi.org/10.1016/j.atmosres.2014.11.023>, 2015.

520 Zhang, B., Wang, Y., and Hao, J.: Simulating aerosol-radiationcloud feedbacks on meteorology and air quality over eastern  
521 China under severe haze conditions in winter, *Atmos. Chem. Phys.*, 15, 2387–2404, [http://doi.org/10.5194/acp-15-2387-](http://doi.org/10.5194/acp-15-2387-2015)  
522 2015, 2015.

523 Zhang, D., and Anthes, R. A.: A high-resolution model of the planetary boundary layer—Sensitivity tests and comparisons  
524 with SESAME-79 data, *J. Appl. Meteorol.*, 21, 1594-1609, 1982.

525 Zhang, R., Li, Q., and Zhang, R.: Meteorological conditions for the persistent severe fog and haze event over eastern China  
526 in January 2013, *Sci. China Earth Sci.*, 57, 26–35, <https://doi.org/10.1007/s11430-013-4774-3>, 2014.

527 Zhong, J., Zhang, X., Dong, Y., Wang, Y., Liu, C., Wang, J., Zhang, Y., and Che, H.: Feedback effects of boundary-layer  
528 meteorological factors on cumulative explosive growth of PM<sub>2.5</sub> during winter heavy pollution episodes in Beijing  
529 from 2013 to 2016, *Atmos. Chem. Phys.*, 18, 247–258, <https://doi.org/10.5194/acp-18-247-2018>, 2018.

530

531 **Table 1.** Typical values of  $z_{0m}$  corresponding to various land-cover types

$z_{0m}$ / m	Land-cover types
5 ~ 50	Mountain (above 100m)
1 ~ 5	The center of large cities, hills or mountain area
0.1 ~ 1	Forests, the center of large towns
0.01 ~ 0.1	Flat grasslands, agricultural fields
$10^{-4} \sim 10^{-3}$	The snow surface, wide water surface, flat deserts
$10^{-5}$	The ice surface

532

533

534

535

**Table 2.** Statistics between the Li and MM5 schemes calculated turbulent flux at Gucheng station.

		Li				MM5			
		MB	NMB	NME	RMSE	MB	NMB	NME	RMSE
Whole	$\tau$	-0.0006	-3.63 %	54.29 %	0.0142	0.0058	34.03 %	63.59 %	0.0143
process	H	-2.2723	-15.69 %	52.73 %	10.9649	-7.2735	-50.22 %	69.68 %	12.7946
Stage 1	$\tau$	0.0021	9.98 %	55.90 %	0.0172	0.0091	43.45 %	66.66 %	0.0169
	H	1.1775	5.79 %	37.87 %	10.5734	-7.1891	-35.34 %	55.70 %	13.1324
Stage 2	$\tau$	0.0013	7.68 %	44.50 %	0.0111	0.0079	45.56 %	56.81 %	0.0121
	H	-4.5752	-33.84 %	50.28 %	9.3995	-10.3924	-76.88 %	81.40 %	13.2553
Stage 3	$\tau$	-0.0024	-13.25 %	59.13 %	0.0144	0.0030	16.72 %	56.34 %	0.0138
	H	1.2818	11.39 %	66.31 %	11.4778	-1.7479	-15.52 %	65.90 %	10.4219

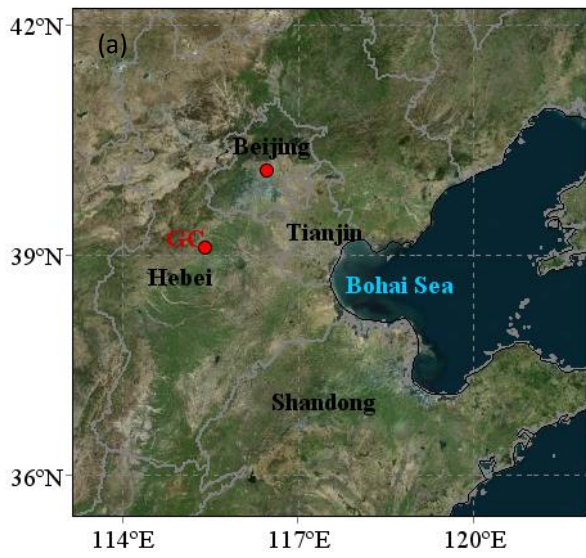
536

\*  $\tau$ : momentum flux; H: sensible heat flux; MB: mean bias; NMB: normalized mean bias; NME: normalized mean error;

537

RMSE: root mean square error. The units of MB and RMSE:  $\mu\text{g m}^{-3}$ .

538



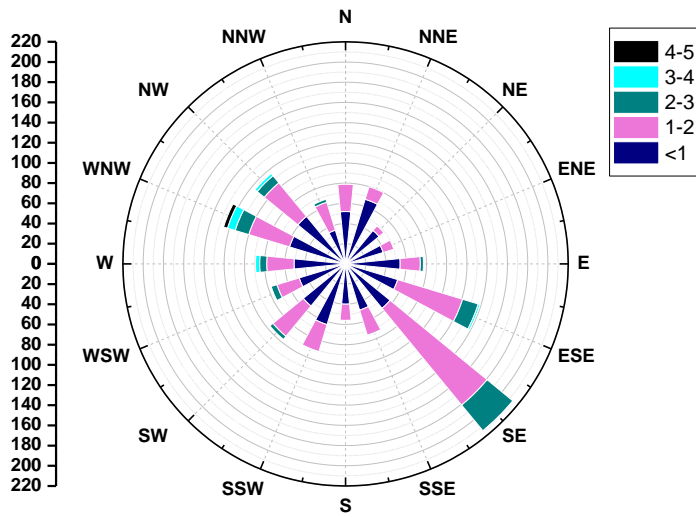
539

540 **Figure 1.** Location (a) and geographical environment (b) at Gucheng station. The map is from Bing Maps.

541

542

543



544

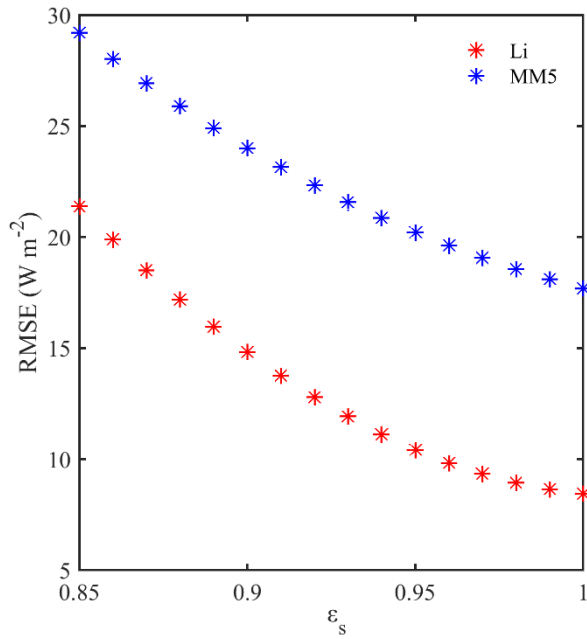
545 **Figure 2.** Wind Rose map at Gucheng station from December 1, 2016, to January 9, 2017.

546

547

548

549



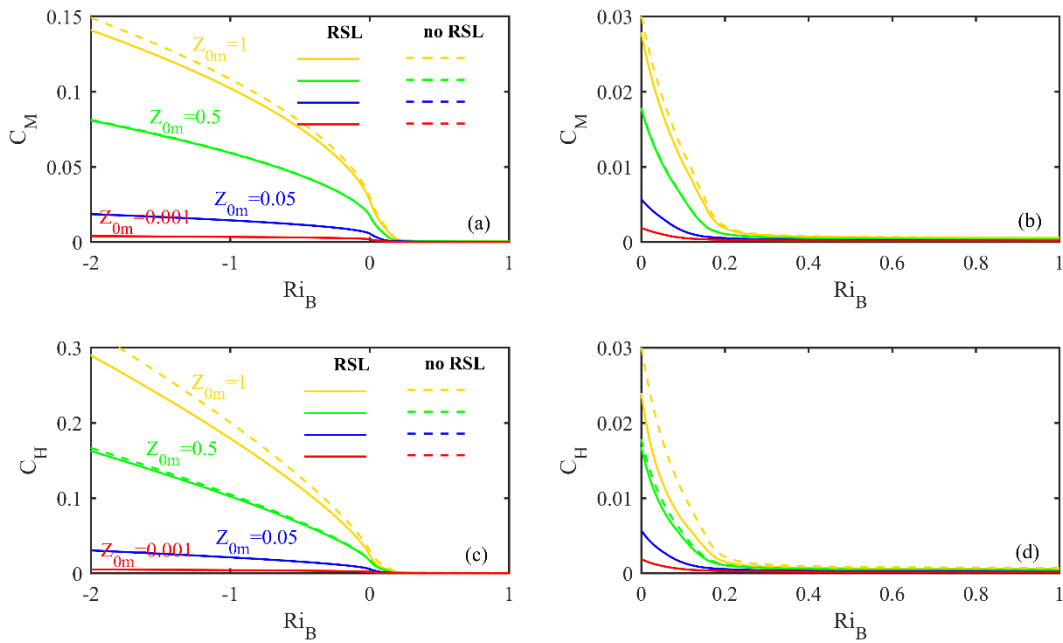
550

551 **Figure 3.** The surface emissivity  $\varepsilon_s$  dependence of RMSE between observed near-neutral heat fluxes and parameterized heat  
 552 fluxes (red for Li and blue for MM5) at Gucheng station.

553

554

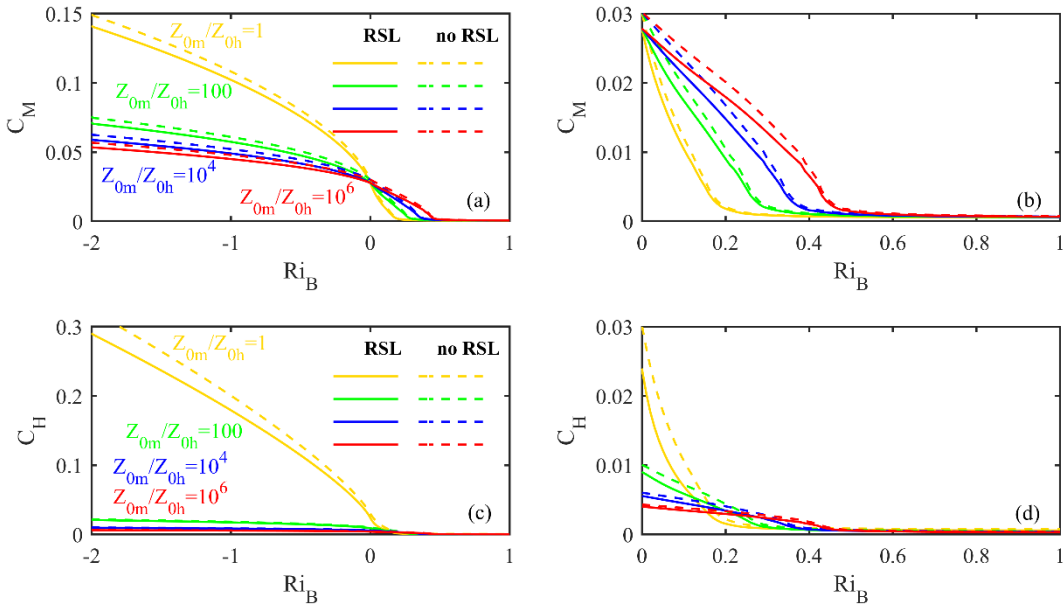
555



556

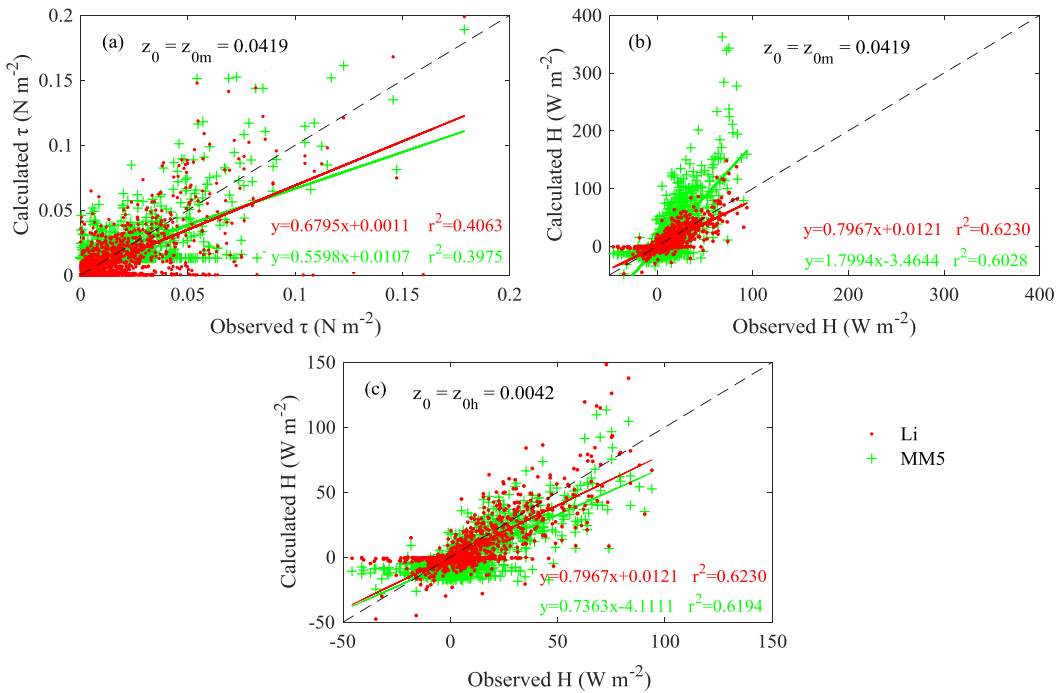
557 **Figure 4.** The relationship between  $C_M(C_H)$  and  $Ri_B$  for different  $z_{0m}$  values and treatment of RSL. Solid lines:  
 558 considering the RSL effect; dotted lines: without the RSL effect.

559



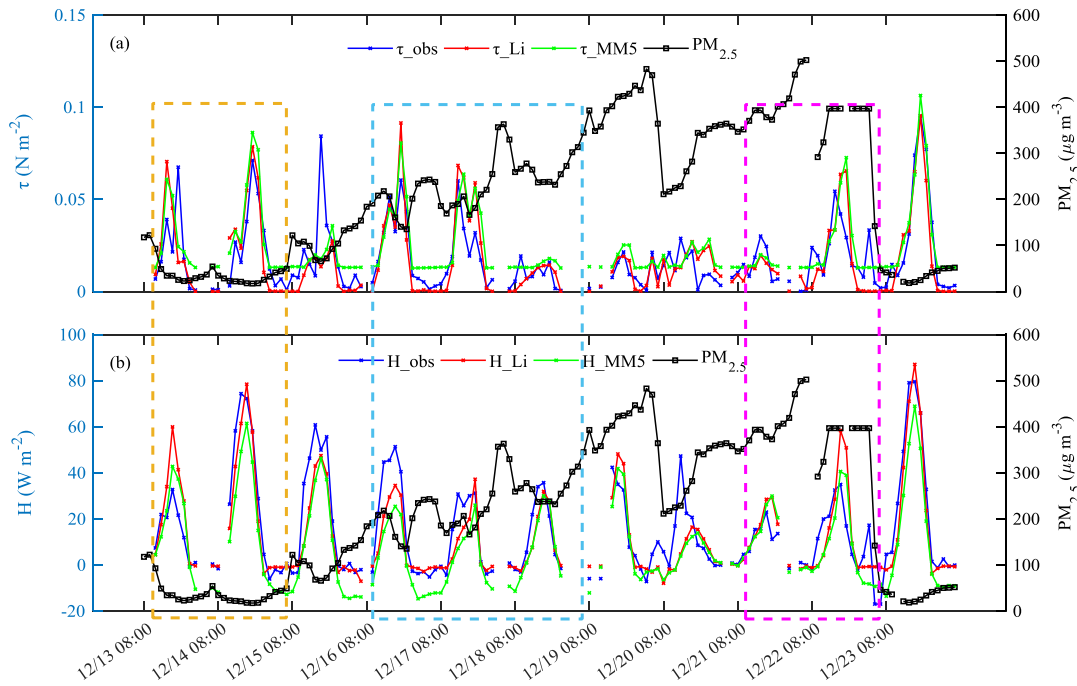
560  
561  
562  
563  
564  
565  
566

**Figure 5.** The relationship between  $C_M$  ( $C_H$ ) and  $Ri_B$  for different ratios of  $z_{0m}$  to  $z_{0h}$  and treatment of RSL. Solid lines: considering the RSL effect; dotted lines: without the RSL effect.



567  
568  
569  
570  
571  
572

**Figure 6.** Comparison of calculated and observed fluxes at Gucheng station from December 1, 2016 to January 9, 2017. (a) Momentum fluxes (MM5:  $z_0 = 0.0419$ ); (b) sensible heat fluxes (MM5:  $z_0 = 0.0419$ ); (c) sensible heat fluxes (MM5:  $z_0 = 0.0042$ ). Red dots: the Li scheme; green plus signs: the MM5 scheme.



575

576

**Figure 7.** Variations of hourly turbulent fluxes and observed  $PM_{2.5}$  at Gucheng station in daytime. (a) Momentum fluxes  $\tau$

577

(blue line: observations; red line: the Li scheme; green line: the MM5 scheme) and  $PM_{2.5}$  concentration (black line); (b) sensible

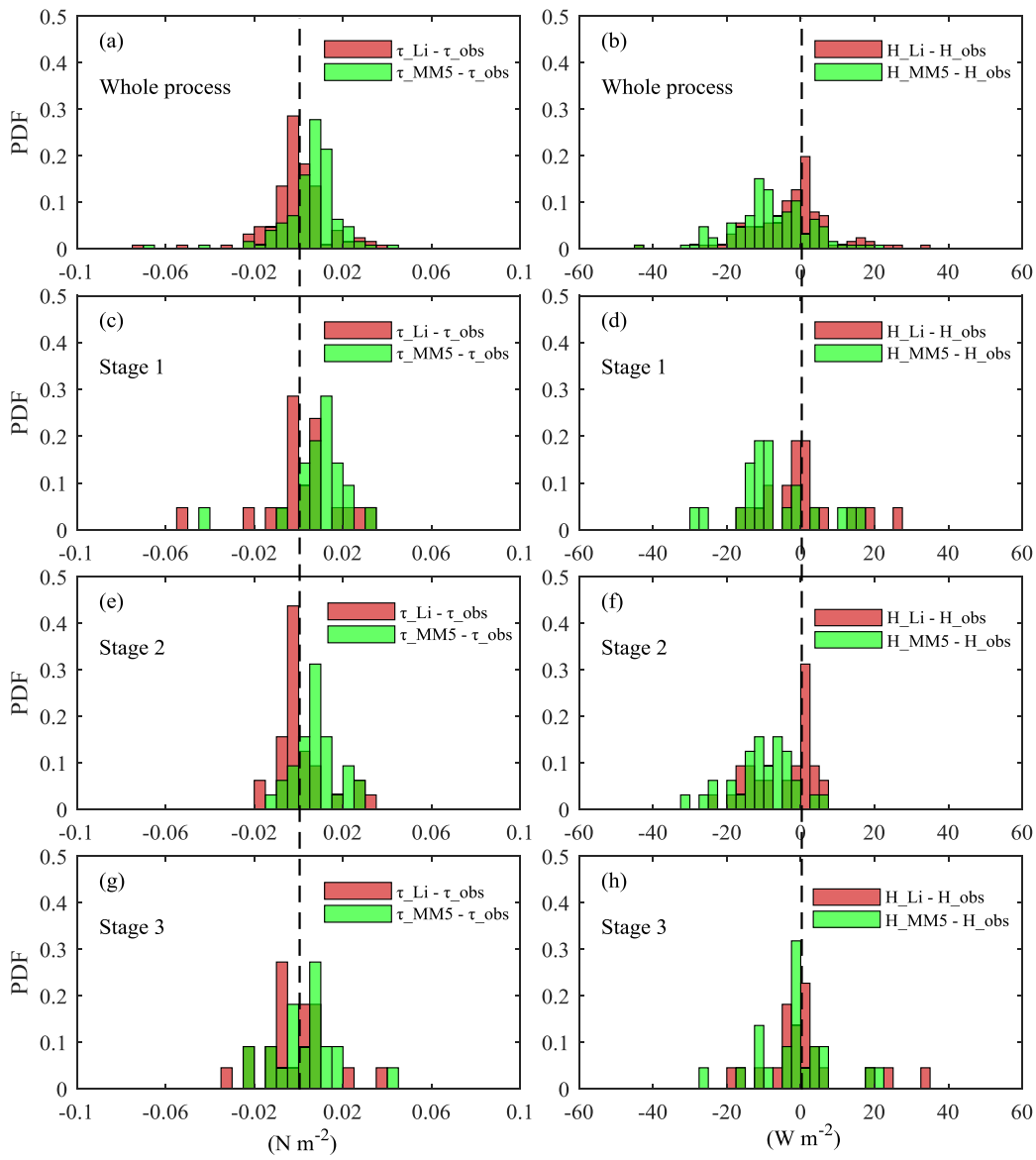
578

heat fluxes  $H$  (the same as  $\tau$ ) and  $PM_{2.5}$  concentration (black line). Yellow box: stage 1; blue box: stage 2; purple box: stage 3.

579

580

581

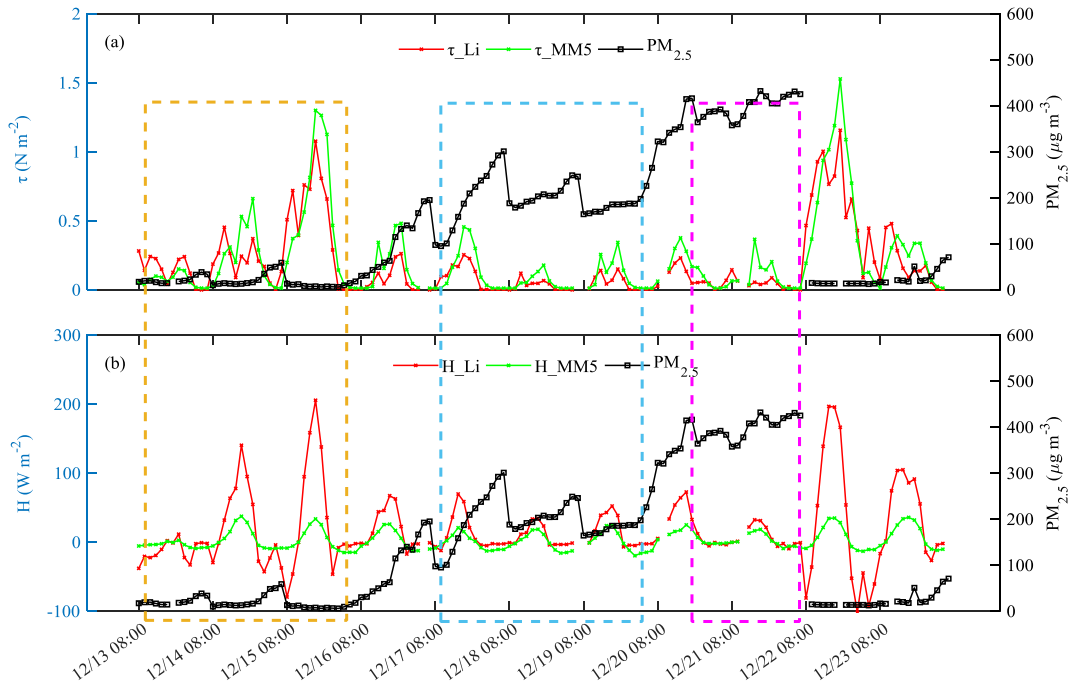


582

583 **Figure 8.** Probability distribution functions (PDF) of the difference between calculated fluxes (momentum fluxes: left; sensible  
 584 heat fluxes: right) by using two schemes (the Li scheme: red bars; the MM5 scheme: green bars) and observations in different  
 585 stages (a-b: whole process; c-d: stage 1; e-f: stage 2; g-h: stage 3).

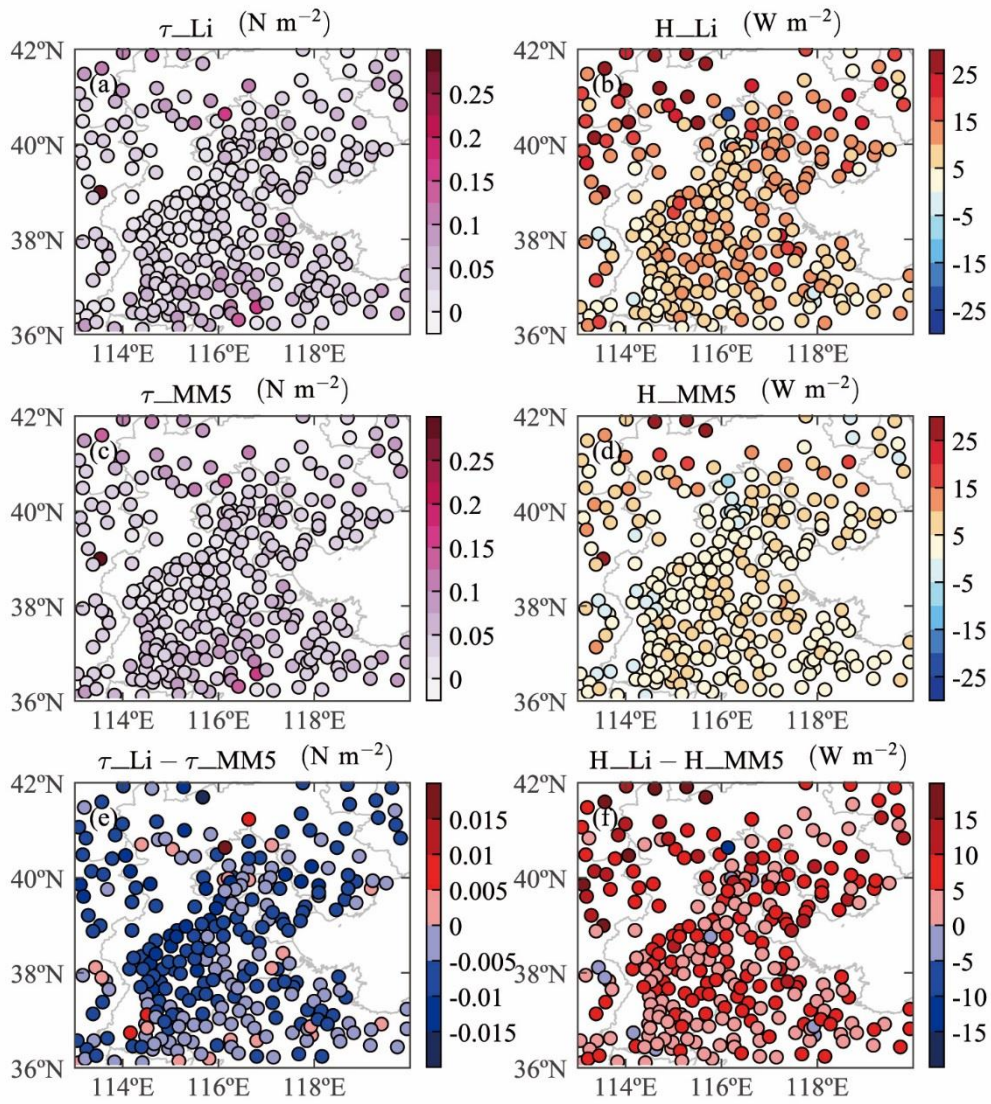
586





587  
 588 **Figure 9.** As in Fig. 7 but for Beijing station.

589  
 590



591  
 592 **Figure 10.** The mean momentum and sensible heat fluxes calculated by using two schemes (a-b: the Li scheme; c-d: the MM5  
 593 scheme) and their difference (e: difference of the momentum fluxes; f: difference of the sensible heat fluxes) in Jing-Jin-Ji  
 594 during the haze episode (December 13 to 23, 2016).